

# Ligand Migration in *Methanosarcina acetivorans* Protoglobin: Effects of Ligand Binding and Dimeric Assembly

Flavio Forti,<sup>†</sup> Leonardo Boechi,<sup>‡</sup> Damian Bikiel,<sup>‡</sup> Marcelo A. Martí,<sup>‡,§</sup> Marco Nardini,<sup>||</sup> Martino Bolognesi,<sup>||</sup> Cristiano Viappiani,<sup>⊥,¶</sup> Darío Estrin,<sup>\*,‡</sup> and F. Javier Luque<sup>\*,†</sup>

<sup>†</sup>Departament de Físicoquímica and Institut de Biomedicina, Facultat de Farmàcia, Universitat de Barcelona, Avinguda Diagonal 643, E-08028, Barcelona, Spain

<sup>‡</sup>Departamento de Química Inorgánica, Analítica, y Química Física, INQUIMAE-CONICET, Facultad de Ciencias Exactas y Naturales, Universidad de Buenos Aires, Ciudad Universitaria, Buenos Aires, Argentina

<sup>§</sup>Departamento de Química Biológica, Facultad de Ciencias Exactas y Naturales, Universidad de Buenos Aires, Ciudad Universitaria, Buenos Aires, Argentina

<sup>||</sup>Dipartimento di Scienze Biomolecolari e Biotecnologie and CIMAINA, Università degli Studi di Milano, I-20131 Milano, Italy

<sup>⊥</sup>Dipartimento di Fisica, Università degli Studi di Parma, Parma, Italy

<sup>¶</sup>NEST, Istituto Nanoscienze-CNR, Italy

**S** Supporting Information

**ABSTRACT:** Protoglobin is the first globin found in *Archaea*. Its biological role is still unknown, although this protein can bind O<sub>2</sub>, CO, and NO reversibly in vitro. The X-ray structure of *Methanosarcina acetivorans* protoglobin (*MaPgb*) has shown that access of ligands to the heme, which is completely buried within the protein matrix, can be granted by two apolar tunnels, which are mainly defined by helices G and B (tunnel 1), and helices B and E (tunnel 2). Here we analyze the structural and dynamical behavior of *MaPgb* through molecular dynamics and computational techniques aimed at shedding light on distinctive features of ligand migration through the tunnels that may be linked to functionality. While tunnel 2 is found to be accessible to diatomic ligands in both deoxygenated and oxygenated forms of the protein, the accessibility of tunnel 1 is controlled through the synergistic effect of both the protein dimeric state and the presence of the heme-bound ligand. Thus, dimerization mainly affects the spatial arrangement of helix G, which influences the shape of tunnel 1. Ligand accessibility through this tunnel is regulated by Phe(145)G8, which can adopt *open* and *closed* conformations. Noteworthy, the ratio between open and closed states is modulated by protein dimerization and more strikingly by ligand binding. In particular, sensing of the ligand is mediated by Phe(93)E11, and the steric hindrance between Phe(93)E11 and the heme-bound ligand alters the structural and dynamical behavior of helices B and E, which facilitates opening of tunnel 1. This functional mechanism provides a basis to understand the finding that ligation favors fast rebinding from ligand binding kinetic to *MaPgb*. Finally, it also suggests that *MaPgb* might be physiologically involved in a ligand-controlled bimolecular chemical process.



## INTRODUCTION

Globins comprise a family of heme-containing proteins found in all kingdoms of life. They have evolved to play a variety of biological roles, such as O<sub>2</sub> transport and storage, NO detoxification, or sensing of diatomic gases.<sup>1–3</sup> Some globins act as monomers under physiological conditions, but in other cases the biologically relevant form involves multimeric species, as illustrated by the prototypical cases of mammalian myoglobin (Mb) and hemoglobin (Hb), respectively.<sup>3–6</sup> From a structural point of view, globins generally adopt a common fold characterized by a 3-over-3 helical sandwich, which contains the low polarity pocket that accommodates the heme group. The heme iron atom is coordinated to a conserved proximal HisF8 residue,<sup>7</sup> leaving the sixth coordination position in the distal side usually free for binding of the exogenous ligand.

Much of the diversity within the globin superfamily has been disclosed by the progresses made in the last two decades, which have worked out novel Hbs with distinct structural and functional features. This can be exemplified by the subgroup of 2/2Hbs, which are typically smaller (around 20–30 residues shorter) than Mb and exhibit a characteristic 2-over-2 sandwich fold.<sup>8,9</sup> 2/2Hbs have been proposed to act as small gas molecule sensors, oxygen carriers, and enzymes. A different globin subgroup includes protoglobin (Pgb) and globin-coupled sensor (GCS) proteins, whose globin domain (~190 amino acids) is bigger than that of Mb.<sup>10–13</sup> Pgb's are the first single-domain GCS-related globins

**Received:** September 5, 2011

**Revised:** October 8, 2011

**Published:** October 10, 2011

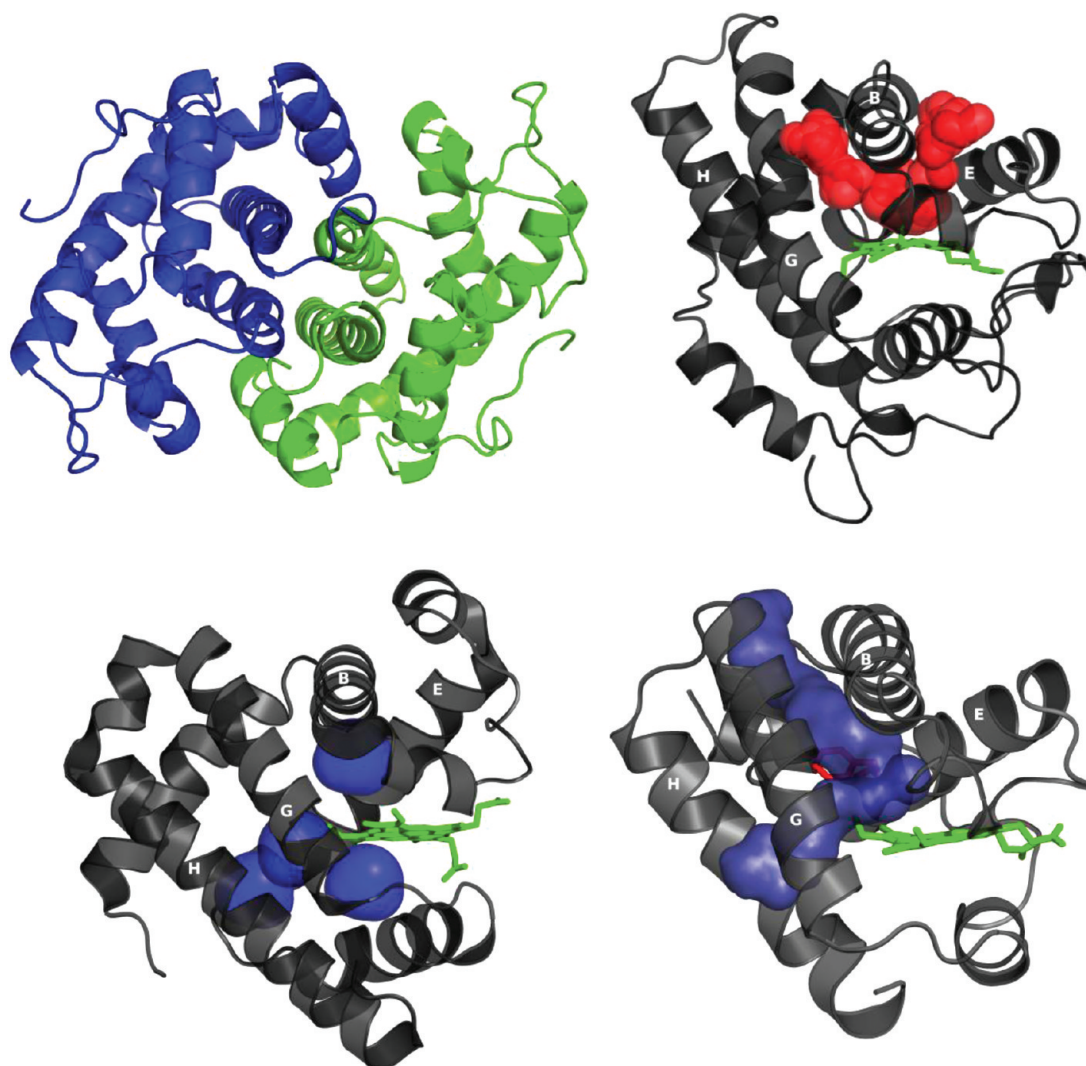


**Figure 1.** View of the 3D structure of dimeric *MaPgb* (PDB entry 2VEE; top-left), which is oriented to show the interface formed by helices G and H. The two tunnels observed in each subunit of *MaPgb* are shown in red (top-right). The tunnels are mainly delineated by helices B/G (tunnel 1) and B/E (tunnel 2). For the sake of comparison, the Xe binding sites (shown in blue) found in sperm whale Mb (PDB entry 1J52) and the internal tunnel formed by two orthogonal branches (shown in blue) in the truncated Hb N from *M. tuberculosis* (PDB entry 1IDR) are shown in the lower panels, respectively (Mb: left; truncated Hb N: right), with the heme group shown as green sticks. To facilitate the comparison of the topological differences between tunnels/cavities, the protein matrix is shown in the same tridimensional orientation.

found in *Archaea*. They can bind  $O_2$ , CO, and NO reversibly in vitro, but their function is still unknown.<sup>11–13</sup>

The X-ray structure of *Methanosarcina acetivorans* Pgb (*MaPgb*) has been recently solved, revealing a number of peculiar structural features.<sup>14</sup> Contrary to most of the known globins, it contains nine helices, as a pre-A helix (named Z) can be clearly distinguished. Other unusual trends are a large distortion of the heme moiety, and its complete occlusion in the protein matrix by the extended CE and FG loops and a 20-residue long N-terminal loop. Access of diatomic ligands to the heme has been proposed to be granted by two tunnels, which are mainly defined by helices B/G (tunnel 1) and B/E (tunnel 2), and whose spatial orientation gives rise to an apolar V-shaped channel (Figure 1). Noteworthy, the topology of these tunnels is a unique feature of Pgb, as it differs from the system of internal cavities found in other globins, such as the set of cavities found in Mb and the orthogonal branches of the tunnel found in 2/2Hbs (exemplified by X-ray structures 1J52 and 1IDR in Figure 1). As many other GCS proteins,

*MaPgb* behaves as a dimer in solution and displays a  $2,086 \text{ \AA}^2$  association interface contributed mostly by residues belonging to helices G and H, which build an intermolecular four-helix bundle, partly to the Z-helix, and to the BC and FG hinges.<sup>14</sup>

These unique structural properties, together with an unusually low  $O_2$  dissociation rate ( $0.092\text{--}0.0094 \text{ s}^{-1}$ ), make *MaPgb* a relevant protein for studies aimed at gaining insight into structure–function relationships within the globin superfamily. To this end, the study of ligand association and dissociation is fundamental to explore the migration properties through the protein matrix. The association rate is mainly determined by ligand migration through the protein matrix, as chemical bonding of the diatomic ligand to the iron atom is in general very fast.<sup>15</sup> Nevertheless, differences in the intrinsic combination to the heme and the formation of specific interactions with protein residues can give rise to differences in the on-rate for ligands such as  $O_2$ , NO, and CO.<sup>16–20</sup> In turn, this process may be affected by transient barriers between dynamically fluctuating cavities or by

gating mechanisms along tunnels.<sup>21–23</sup> Conversely, the dissociation rate is mainly determined by the interactions that stabilize the heme-bound ligand.<sup>15</sup> In general, low  $k_{\text{off}}$  values can be ascribed to the presence of distal site residues that form hydrogen bonds with the ligand, thus stabilizing the bound state. After thermal breaking of the heme-bound ligand, barriers for migration through the protein matrix could also affect the dissociation rate.

In this study we explored the structural and dynamical behavior of *MaPgb* in order to examine the distinctive features of ligand migration through the two tunnel traversing the interior of the protein. In particular, attention was paid to the effect played by both dimerization and ligand binding on the migration properties. To this end, molecular dynamics (MD) simulations were performed for the protein in its monomeric and dimeric forms in order to explore the effect of structural changes promoted by protein assembly on ligand migration. In addition, simulations of the two assembly states (monomer and dimer) were carried out considering the deoxygenated and oxygenated forms of the protein. The migration properties were examined by different computational techniques, including essential dynamics, implicit ligand sampling (ILS), and steered molecular dynamics (SMD) calculations. The analysis of the ligand migration properties will be used to discuss the functional implications for *MaPgb*.

## METHODS

**System Setup.** The initial structure for MD simulations of the monomeric and dimeric species of *MaPgb* in the oxygenated state was built up from the X-ray crystallographic structure of the O<sub>2</sub>-bound protein (PDB code 2VEB).<sup>14</sup> In turn, the ligand free crystal structure (PDB code 2VEE)<sup>14</sup> was used to simulate the unbound form. The two X-ray structures of *MaPgb* are found as dimers and exhibit a similar spatial arrangement.

The starting structures were immersed in a pre-equilibrated octahedral box of TIP3P water molecules.<sup>24</sup> All systems were simulated at constant pressure (1 atm) and temperature (298 K) using periodic boundary conditions and the particle mesh Ewald (PME)<sup>25</sup> method for treating long-range electrostatic interactions. The SHAKE algorithm<sup>26</sup> was used to keep bonds involving hydrogen atoms at their equilibrium length. A 1 fs time step was used for the integration of Newton's equations. The parm99SB force field<sup>27</sup> was used for the protein residues. For the heme, we adopted the parameters developed by our group and thoroughly tested in previous works,<sup>28,29</sup> although slight adjustments mainly involving angles and torsions were introduced to account for the unusual high distortion of the heme found in the X-ray structures (see Table S1 in Supporting Information).

All simulations were performed with the PMEMD module of the AMBER9 program.<sup>30</sup> Equilibration protocols consisted of performing an initial optimization of the initial structures, followed by a slow heating up to the desired temperature. Energy minimization was performed in three subsequent steps where hydrogen atoms, water molecules, and finally the whole system were minimized. Heating was performed in successive 50 ps runs where the temperature was gradually increased from 100 to 298 K in four steps at constant volume, followed by an additional step run at constant pressure for 100 ps. Then, a series of 500 ns MD simulations (at 298 K and 1 atm) were run for the monomeric and dimeric protein in both deoxygenated and oxygenated states, covering a total simulation time of 2  $\mu$ s. The use of extended MD trajectories is necessary to allow the conformational rearrangements associated with the formation/breaking of the dimer into

separate monomers in aqueous solution (see below). The analysis of the trajectories was performed by using frames collected every 1 ps during the production runs.

**Ligand Migration Profiles.** In order to examine the migration of ligands through the protein matrix, we have identified the preferred docking sites for the oxygen molecule and determined the migration free energy profiles along the protein tunnels that connect the solvent with the distal site. To this end, we first performed ILS calculations,<sup>31</sup> where the free energy of placing a probe ligand at a given position is estimated using eq 1.

$$G_{\text{ILS}}(r) = -k_{\text{B}}T \ln \sum_{n=1}^N \sum_{k=1}^C \frac{e^{-\Delta E_{n,k}(r)/k_{\text{B}}T}}{NC} \quad (1)$$

where  $N$  is the number of protein states,  $C$  stands for the number of equally probable ligand orientations, and  $\Delta E_{n,k}$  is the protein–ligand interaction energy.

ILS computations were performed using a three-dimensional (3D) grid that encompasses the whole protein with a 0.5 Å resolution. Moreover, 50 orientations of the probe molecule per grid point and a total set of 5000 snapshots taken every 2 ps were considered to determine the free energy at each grid point. This was repeated for different 10 ns windows along the simulations. Inspection of the free energy isosurfaces depicted on the 3D grid points allowed us to identify potential docking sites and migration paths through the protein matrix.

The identification of pockets and channels derived from ILS computations relies on the use of snapshots taken from the trajectory run for the free protein. Nevertheless, although this computational approach takes into account the intrinsic motions of the free protein, the main limitation is the lack of an explicit description of the ligand, whose migration through the protein matrix should be coupled with the structural fluctuations due to protein dynamics. Accordingly, the suitability of the ILS method is linked to the assumption that the presence of the ligand does not affect the local and/or global dynamical behavior of the protein, or alternatively that the ligand interacts weakly with the protein and hence the dynamical interplay between ligand migration and thermal fluctuations of internal cavities can be omitted. Clearly, this assumption permits the ILS technique to provide a very fast determination of the free energy landscape for the motion of the ligand, which can be suitable for a qualitative understanding of ligand migration, but can be more questionable regarding the energetics of the free energy surface (see ref 32 for a recent critical discussion).

To further refine the free energy profiles, constant velocity multiple SMD simulations were run to examine the migration of O<sub>2</sub> through the tunnels using Jarzynski's equality (eq 2),<sup>33</sup> which relates the free energy with the irreversible work performed upon steering the probe along the reaction coordinate.

$$e^{-\Delta A(\xi)/k_{\text{B}}T} = \langle e^{-W(\xi)/k_{\text{B}}T} \rangle \quad (2)$$

where  $\Delta A$  stands for the change in free energy along the along the reaction coordinate ( $\xi$ ), and  $W(\xi)$  is the external work performed on the system as it evolves from the initial to the final state computed by integrating the force acting on the steering potential along the reaction coordinate.

The steering potential forces the motion of the probe with constant velocity ( $v$ ) along the reaction coordinate (eq 3). In the present study, the reaction coordinate  $\xi$  was chosen as the

iron–ligand distance, the force constant was  $200 \text{ kcal mol}^{-1} \text{ \AA}^{-1}$ , and the pulling velocity was  $0.025 \text{ \AA ps}^{-1}$ .

$$E(r) = k[r - (\zeta_0 + v\Delta t)]^2 \quad (3)$$

To compute the free energy profile of ligand migration along a selected tunnel, we have adopted the computational scheme used in previous studies for truncated hemoglobins by our group.<sup>28,29,34</sup> Briefly, at least 20 SMD simulations were run pushing the ligand through the tunnel from the solvent toward the iron. Due to the expensiveness of SMD computations, the free energy profile was determined for only one of the subunits. At this point, it is worth noting that similar results are expected for each of the two subunits, as noted from the high similarity between the ILS free energy isocontours determined for the two subunits of the dimeric protein (see below). The starting snapshot for each SMD was taken from the final structure of an equilibrated MD simulation run with the ligand placed at a fixed distance from the iron. Typically, those distances were chosen from the preferred docking sites found during the motion of the free diatomic ligand in short MD simulations.

## RESULTS AND DISCUSSION

**Overall Structural Analysis of MaPgb.** Extended MD simulations were run to explore the structural integrity and flexibility of MaPgb. We aimed to capture not only the fluctuations that modulate the shape and size of cavities and tunnels, but more importantly to examine the differences found for monomeric and dimeric forms of MaPgb, as well as the effect played by the presence of the ligand ( $\text{O}_2$ ) bound to the heme. Accordingly, a series of 500 ns MD simulations were run for deoxygenated ligand-free (Pgb-deoxy) and oxygenated (Pgb- $\text{O}_2$ ) forms of the protein treated either as a monomer (MPgb) or a dimer (DPgb). As will be discussed below, the use of very extended trajectories is necessary to account for the structural rearrangements observed in certain helical segments along the trajectories, and thus to obtain an adequate sampling of the equilibrated systems.

For all the simulations, the time evolution of the root-mean-square deviation (rmsd; determined relative to the X-ray structure; see Figure S1 in Supporting Information) was computed for the backbone atoms of the protein core (residues 23–189), thus neglecting the contributions due to N- and C-terminal tails, which showed higher mobility compared to the core of the protein. The rmsd profile for DPgb-deoxy is stable at around  $1.5 \text{ \AA}$  after the first 50 ns. A slightly lower value (rmsd of  $1.3 \text{ \AA}$ ) is obtained for DPgb- $\text{O}_2$ , although this value is achieved after a progressive increase in the rmsd profile during the first 220 ns. The rmsd determined for the monomers is larger than the value calculated for the dimeric forms, as it amounts to  $1.8$  and  $2.2 \text{ \AA}$  for MPgb-deoxy and MPgb- $\text{O}_2$  at the end of the trajectories. This finding is not unexpected, as both X-ray structures (PDB codes 2VEB and 2VEE) used to build up the simulated systems correspond to dimeric forms of the protein.

The preceding results suggest that dissociation of the dimer into separate monomers does not promote a substantial alteration in the overall fold of the protein. However, the larger rmsd found for the monomers reveals the occurrence of local rearrangements in certain structural elements upon dissociation of the dimer. In this respect, a detailed structural analysis of the distinct helical segments showed that there is a relevant displacement of helix G (and to a lower extent of helix H) in MPgb-deoxy compared to the X-ray crystal structure (PDB entry 2VEE; Figure 2).

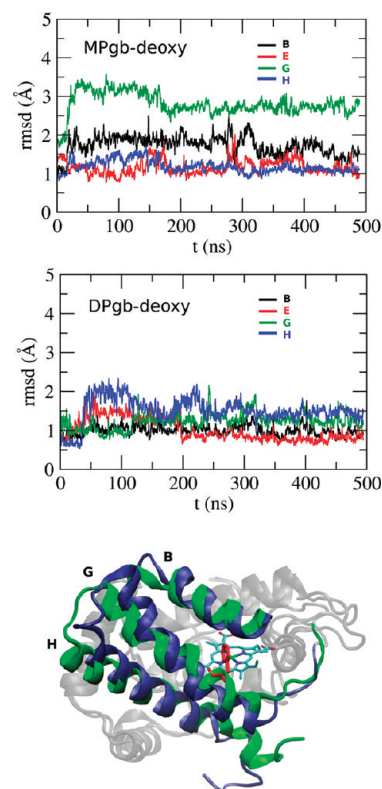


**Figure 2.** Time (ns) evolution of the rmsd (Å) of the backbone atoms in selected helical segments of the deoxygenated (top) monomer and (middle) dimer determined relative to the X-ray structure (PDB entry 2VEE). (Bottom) Superposition of helices B, G, and H in the final snapshots of simulations run for monomer (green) and dimer (blue) in the deoxygenated state. Phe(145)G8 and heme are shown as red and atom-colored sticks.

Thus, whereas the rmsd of helix G amounts to  $\sim 1.2 \text{ \AA}$  in the dimer (a value comparable with the rmsd of other helices), the rmsd is enhanced to about  $2.9 \text{ \AA}$  in the monomer (Figure 2). Since helix G is directly involved in defining the interface between the interacting units in the dimeric form of MaPgb, dissociation of the dimer increases dramatically the exposure of helix G to the aqueous solvent, thus facilitating the conformational relaxation in the monomer compared to the dimer. Since helix G, together with helix B, defines the shape of tunnel 1 (see Figure 1), conformational changes in helix G might have a direct effect on ligand accessibility through this tunnel (see below).

Strikingly, when the same analysis is performed for the oxygenated forms of the protein in both monomeric and dimeric forms, the largest rmsd (determined relative to the X-ray crystal structure; PDB entry 2VEB) is mainly found for helices B, E, and G (Figure 3). In DPgb- $\text{O}_2$ , the structural rearrangement primarily affects helix B, whose rmsd (around  $2.2 \text{ \AA}$ ) is sensibly larger than that determined for helices E and G (around  $1.6 \text{ \AA}$ ). Nevertheless, in MPgb- $\text{O}_2$ , the structural rearrangement primarily affects helices E (rmsd close to  $2.8 \text{ \AA}$ ) and G (around  $2.2 \text{ \AA}$ ). As for the analysis made for the deoxygenated monomer and dimer (see above and Figure 2), the conformational relaxation of helix G is not unexpected and can be explained by the dissociation of the dimer. However, the results for the oxygenated protein suggest that the heme-bound ligand exerts additional effects, which primarily affect the structural properties of helices

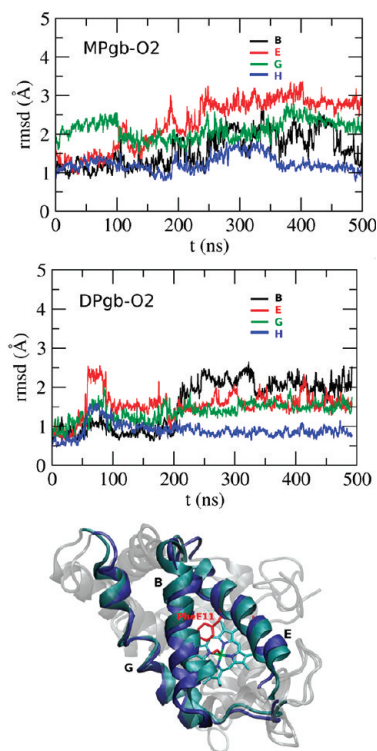


**Figure 3.** Time (ns) evolution of the rmsd (Å) of the backbone atoms in selected helical segments of the oxygenated (top) monomer and (middle) dimer determined relative to the X-ray structure (PDB entry 2VEB). (Bottom) Superposition of helices G, B, and E in the final snapshots of simulations run for deoxygenated (blue) and oxygenated (cyan) states of the dimer. Phe(93)E11 and heme are shown as red and atom-colored sticks.

B and E (see Figure 3 bottom). Since helices B and E define the walls of tunnel 2, these findings suggest questions about the potential role played by the heme-bound ligand on the accessibility to the tunnels.

It is worth noting that the structural fluctuation of helices B and E in the oxygenated protein is associated with a drastic change in the dynamical behavior of the protein triggered upon ligand binding, as noted in the essential motions of the protein skeleton determined by diagonalizing the positional covariance matrix for the backbone atoms of the protein core.<sup>35,36</sup> The calculated eigenvalues decrease in magnitude smoothly, thus indicating that a variety of motions determine the structural flexibility of the protein backbone. However, whereas the first 10 principal components account for around 50% of the structural variance, the first eigenvalue alone describes between 13% and 19% of the structural fluctuations. The nature of this single essential mode is drastically different in the deoxygenated and oxygenated forms of the protein (Figure 4). In the deoxygenated species it mainly involves displacements of helix A and those segments of helices G and H close to helix A. In contrast, the first essential mode for the heme-bound O<sub>2</sub> protein mainly involves the displacement of helices B and E. Since helix B contributes to define the shape of tunnels 1 and 2, its increased flexibility might be relevant to facilitate the migration of ligands to/from the heme cavity.

On the basis of these findings, we can conclude that both dissociation of the dimer and the presence of the heme-bound ligand promote distinctive structural and dynamical alterations in helices B, E, and G of *MaPgb*. Because these helical segments

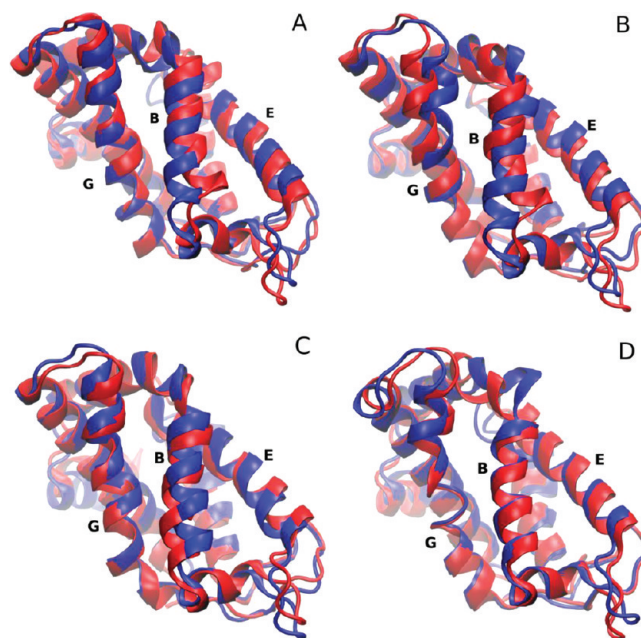


**Figure 4.** Representation of pairs of snapshots that represent the deformations of the protein backbone due to the first essential mode for (A) MPgb-O<sub>2</sub>, (B) DPgb-O<sub>2</sub>, (C) MPgb-deoxy, and (D) DPgb-deoxy forms of *MaPgb*.

delineate the two tunnels in the protein matrix, it can be expected that ligand migration is likely affected by both the dimeric assembly of the protein and by the binding of ligands to the heme cavity. In turn, the same findings prompt two main questions: (i) how the presence of the ligand can be sensed by the protein and affect the structural and dynamical behavior of helices B and E, and (ii) how alterations of the helical properties triggered by both dimerization and ligand binding affect the accessibility of ligands through the tunnel.

**Structural Changes in the Distal Cavity.** To answer these questions, we have first analyzed the structural changes induced in the distal cavity upon dissociation of the dimer and upon binding of O<sub>2</sub> to the heme.

The binding of ligands to the heme is generally sensed via formation of hydrogen bonds in the heme cavity. Hydrogen-bonding with distal residues not only contributes to stabilize the heme-bound ligand, but can also promote structural and dynamical changes in the protein as, for instance, reported for the 2/2HbN in *M. tuberculosis* (*MtHbN*), where the alteration of the hydrogen-bonding network formed by polar residues upon O<sub>2</sub> binding to the heme changed the main essential motions of the protein skeleton.<sup>37,38</sup>

Inspection of the X-ray structure of *MaPgb*, however, shows that there is no hydrogen bonding stabilization of the heme-bound O<sub>2</sub> in the distal cavity. The most plausible residue that could stabilize the ligand is Tyr(61)B10, but its hydroxyl group is too far from the heme-bound O<sub>2</sub> in PDB entry 2VEB (distance OH(TyrB10)⋯O(O<sub>2</sub>) of 5.26 Å), and no water molecules were found to mediate the interaction between Tyr(61)B10 and O<sub>2</sub>. Nevertheless, thermal fluctuations could facilitate the local reorientation of the phenolic group to enable hydrogen bonding with the ligand.

The potential involvement of distal hydrogen bonds in assisting the O<sub>2</sub> binding was examined based on the time evolution of

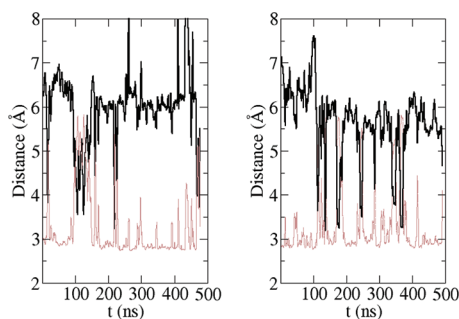


**Figure 5.** Time (ns) evolution of OH(TyrB10)···O(O<sub>2</sub>) (black) and OH(TyrB10)···O(LeuE4) (gray) distances (Å) for the oxygenated forms of (left) monomeric and (right) dimeric MaPgb. For the dimer, only the distances determined for subunit A are shown. Similar results stand for subunit B.

the distance between the hydroxyl oxygen of TyrB10 and O<sub>2</sub> in the oxygenated forms of both monomeric and dimeric MaPgb (Figure 5). Although there are few attempts to form a hydrogen bond with the heme-bound O<sub>2</sub>, the distance OH(TyrB10)···O<sub>2</sub> (O<sub>2</sub>) is generally close to 6 Å. In fact, most of the time Tyr(61)B10 is hydrogen bonded to the carbonyl oxygen of Leu(86)E4. Similarly, analysis of the snapshots ruled out a significant stabilization due to water-mediated bridges with Tyr(61)B10. Overall, the present results exclude a significant contribution of Tyr(61)B10 in stabilizing the ligand. In turn, this finding supports the idea that the very low O<sub>2</sub> dissociation rate found in MaPgb has to be ascribed mostly to the strong distortion of the Pgb heme, as suggested by recent *in silico* analysis.<sup>39</sup>

The absence of hydrogen bonding potentially stabilizing the heme-bound O<sub>2</sub> prompted us to search for contacts between the ligand and vicinal residues in the distal cavity. To this end, we have analyzed the distribution of distances from the iron atom in order to adopt a common frame for both deoxygenated and oxygenated forms of the protein. On the basis of this analysis, two aromatic residues, Phe(145)G8 and Phe(93)E11 (see Figure S2 in the Supporting Information), emerged as putative candidates in sensing the presence of the heme ligand in MaPgb. It is worth noting that in the X-ray structure of oxygenated MaPgb, Phe(93)E11 was found to be the closest residue to O<sub>2</sub> (at 3 Å), with its side chain affected by conformational disorder. On the contrary, Phe(93)E11 adopts a defined conformation in the absence of the heme ligand.<sup>14</sup>

Regarding Phe(145)G8, the average distance determined from the phenyl ring to the iron atom is 4.9 Å for MPgb-deoxy. This value is notably smaller than that found in the X-ray structures, as the closest distance from the side chain of Phe(145)G8 to the iron atom is close to 6 Å. In keeping with the above considerations, the shorter distance found in the MPgb-deoxy simulation may be ascribed to the structural rearrangement of helix G after dissociation of the dimer. More importantly, the monomeric species appears to respond to the heme-bound O<sub>2</sub>, as noted by the increase of the average distances separating the phenyl ring and the iron atom (from 4.9 Å in MPgb-deoxy to 6.0 Å in MPgb-O<sub>2</sub>; see Figure 6). In contrast, such ligand-induced response is remarkably smaller in the dimeric species, as noted in the similar range of average distances (from 6.4 to 6.7 Å) determined for DPgb-deoxy and DPgb-O<sub>2</sub> (Figure 6). Thus, dimerization affects the location of Phe(145)G8 in the distal cavity, which can be ascribed to the spatial rearrangement of

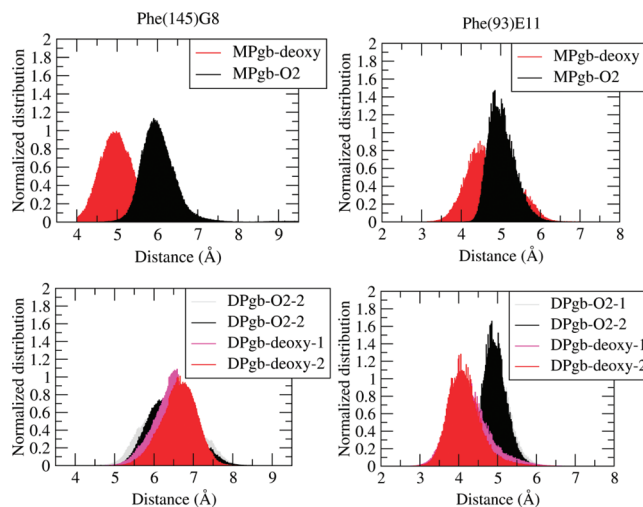


**Figure 6.** Distribution of closest distances between the side chain of (left) Phe(145)G8 and (right) Phe(93)E11 from the heme iron. The distances are determined for both (top) monomeric (MPgb) and (bottom) dimeric (DPgb) species in deoxygenated and oxygenated states. For the dimers the values determined for the two interacting subunits are denoted with “1” and “2”.

helices G and H at the interface between subunits. However, the friction between those helices at the interface reduces the sensitivity of Phe(145)G8 to the presence of the ligand in the dimer relative to the isolated monomer.

Contrary to Phe(145)G8, sensitivity response of Phe(93)E11 to the heme-bound ligand is consistently observed in both monomeric and dimeric forms of MaPgb (Figure 6). In both MPgb-deoxy and DPgb-deoxy the distance of the Phe(93)E11 side chain to the iron atom, which ranges on average from 4.0 to 4.5 Å, increases upon binding of O<sub>2</sub>. Such an increase is about 0.5 Å when the monomeric forms are considered, but it reaches 1.1 Å in the case of the dimeric species. Thus, irrespective of the assembly state (monomer versus dimer) of the protein, the presence of the heme-bound ligand introduces steric hindrance onto the side chain of Phe(93)E11.

Overall, these findings suggest that the ligand sterically collides with the side chain of Phe(93)E11 and contributes not only to the structural change observed in helices B and E (Figure 3), but also to a perturbation of the dynamical motion of these helical segments (Figure 4). Notably, these trends resemble the large-scale conformational change detected both theoretically<sup>35</sup> and experimentally<sup>36</sup> in MthbN. However, whereas in this latter protein the binding is sensed through alteration in the network of hydrogen bonds formed by TyrB10 and GlnE11 in the distal cavity, steric hindrance appears to mediate the ligand sensing properties in MaPgb.

As a final remark, it is worth noting that functionally relevant residues in other globins do not appear to play a crucial role in MaPgb. For instance, PheE15 has been described as a gate residue in MthbN,<sup>35</sup> regulating the access of diatomic ligands through the long branch of the protein matrix tunnel in the oxygenated form of this 2/2Hb. However, MaPgb does not display a similar tunnel, and the E15 position is occupied by an Ile residue that does not appear to play a crucial role. Similarly, since the CD loop, together with the FG loop and the N-terminal extension completely bury the heme, the HisE7 ligand gating mechanism proposed for Mb cannot be sustained in MaPgb,

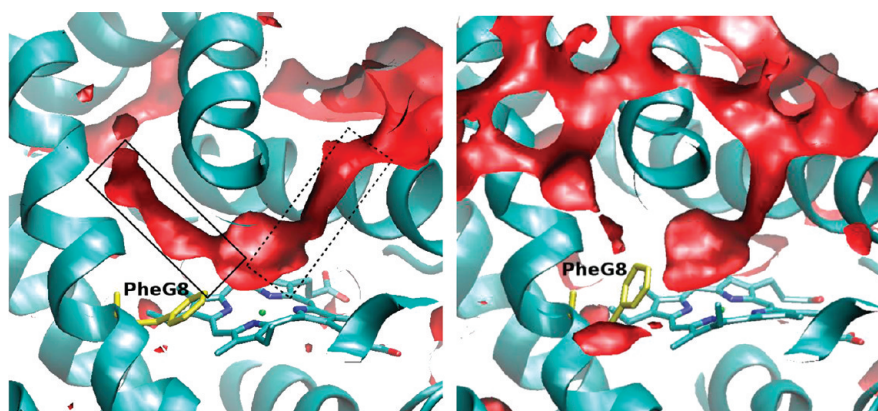


**Figure 7.** Free energy isosurfaces used to delineate tunnels 1 and 2 for DPgb-deoxy. Whereas tunnel 2 (enclosed in dashed line) is open along the trajectory, tunnel 1 (enclosed in solid line) is found in both open (left) and closed (right) states depending on the conformation of Phe(145)G8 (shown as yellow sticks). Heme is shown in atom-colored sticks.

where, additionally, a Val residue is found at the E7 site. Thus, simulation of structure and dynamics in the distal site suggest that in MaPgb the residues mainly involved in functional ligand recognition are Phe(145)G8 and Phe(93)E11, thus at striking difference from ligand binding models known for other globins.

**Ligand Migration.** In order to explore the impact of the structural and dynamical rearrangements on the ligand migration properties of MaPgb, we have analyzed the structural and energetic features of tunnels 1 and 2.

The accessibility of ligands through tunnel 1 seems to be regulated by the side chain of Phe(145)G8, which is found in two main conformations along the MD trajectories (see below). The two conformations can be characterized by the dihedral angle  $N-C_{\alpha}-C_{\beta}-C_{\gamma}$ , which adopts values at  $270^{\circ}$  and  $210^{\circ}$ . The former value reflects the conformation found in the X-ray crystallographic structures ( $267^{\circ}$  in 2VEB, and varying from  $265^{\circ}$  to  $270^{\circ}$  in the eight independent protein molecules present in the asymmetric unit of 2VEE). In this conformational state migration of a diatomic ligand through tunnel 1 is not hindered. On the contrary, in the second conformation the phenyl ring protrudes into the tunnel, where it would hamper the migration of ligands. The impact of the conformational state adopted by Phe(145)G8 on the accessibility of diatomic ligands through tunnel 1 is clearly reflected in the free energy isosurfaces derived from ILS simulations (Figure 7; see also Figure S3 in the Supporting Information). In the following, these two conformations will be denoted “open” and “closed”, respectively.

The relative population of the two conformations accessed by Phe(145)G8 depends on both the assembly state of the protein and on the presence of the ligand in the distal cavity (Figure 8; see also Figure S4 in Supporting Information). Thus, Phe(145)G8 side chain remains in the closed state during the last 250 ns of the trajectories collected for both the deoxygenated (99.9% closed) and oxygenated (98% closed) states of the monomeric protein. Dimerization of the protein promotes a slight increase in the population of the open state, which is found to populate between 5% and 8% in the two subunits of DPgb-deoxy. Remarkably, this trend is significantly enhanced upon binding of  $O_2$  to the distal cavity, since about 25% of the structures sampled in the last 250 ns of the trajectory are found in the open state. On the basis of such results, it can be proposed that (i) binding of  $O_2$  is not sufficient to enhance the accessibility through tunnel 1 in MPgb, and that (ii) dimerization is necessary

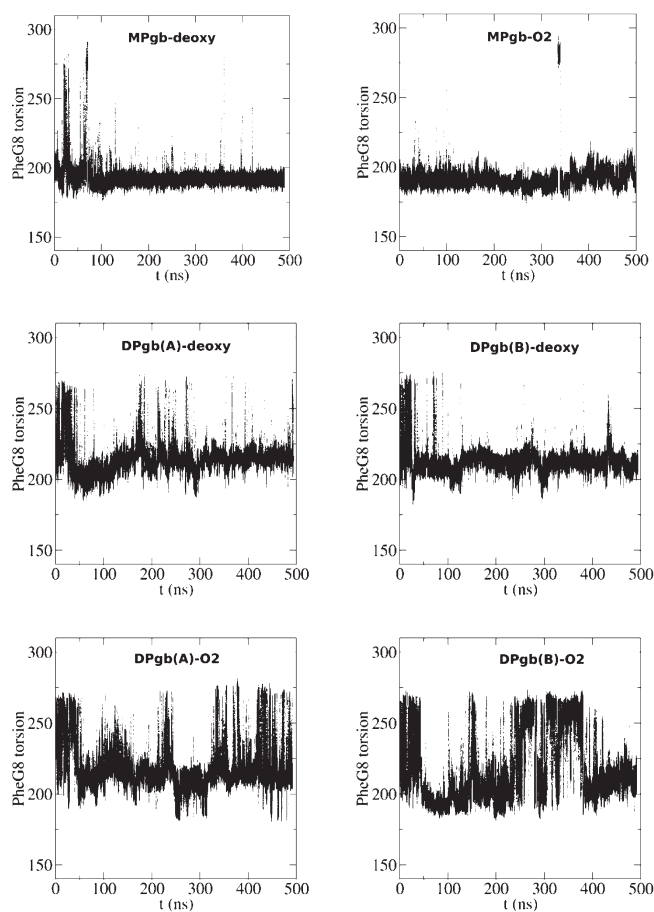


**Figure 8.** Time (ns) evolution of the Phe(145)G8  $N-C_{\alpha}-C_{\beta}-C_{\gamma}$  torsion for (top-left) the MPgb-deoxy, (top-right) MPgb- $O_2$ , (middle) the two subunits (A and B) in the deoxygenated dimer, and (bottom) the two subunits in the oxygenated dimer.

to facilitate the opening of tunnel 1. Moreover, it is worth noting that the enhanced conformational fluctuations of helix B triggered by  $O_2$  binding should also facilitate ligand migration through tunnel 1 (see above).

In contrast to the preceding results, tunnel 2 is found to be accessible irrespective of the presence of heme-bound ligand and

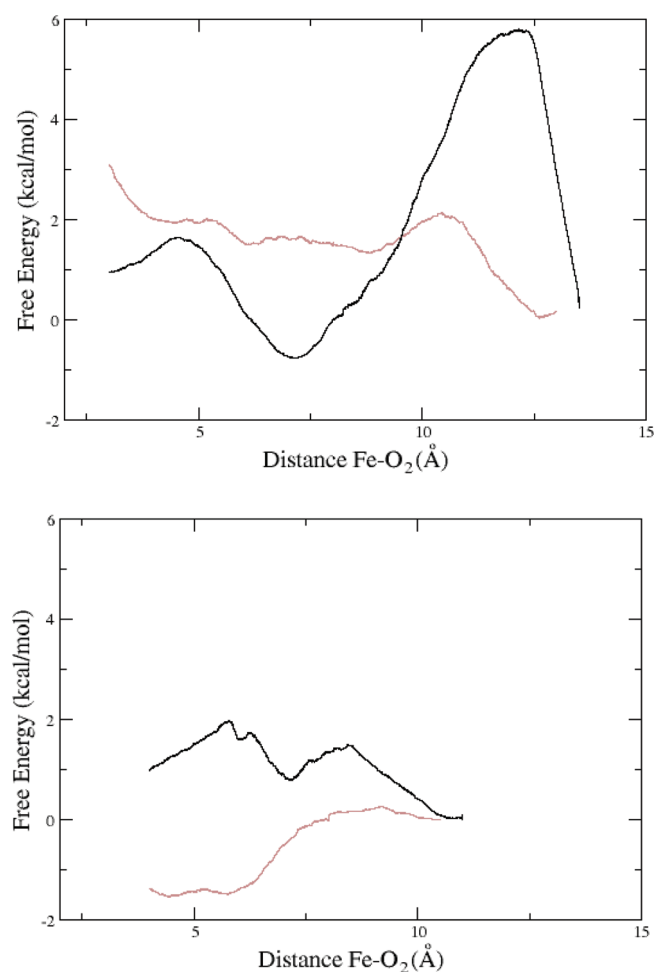


**Figure 9.** Free energy profiles for  $O_2$  migration through (top) tunnel 1 and (bottom) tunnel 2. The profiles are shown for the deoxygenated protein in monomeric (black) and dimeric (gray) states.

of the monomeric/dimeric state of the protein, as noted in the ILS profiles shown in Figure 7 (see also Figure S3 in the Supporting Information). This finding suggests that *MaPgb* might be involved in a ligand-controlled bimolecular chemical process, according to which a small ligand could access the heme cavity through tunnel 2, while a second ligand would diffuse to the distal cavity in the dimeric protein through tunnel 1 (an effect that could be associated with increased flexibility of helix B triggered by the presence of the heme-bound ligand; see Figures 3 and 4). Such a mechanism would not apply to *MPgb*, where tunnel 1 would primarily remain in a closed state (Figure 8).

To further check the relevance of *MaPgb* dimeric assembly, SMD computations were performed to determine the potential of mean force (PMF) for the migration of  $O_2$  through tunnels 1 and 2 using Jarzynski equation (Figure 9). The PMF profile determined for tunnel 1 in *MPgb*-deoxy shows the existence of a high and wide barrier (ca. 6 kcal/mol) at about 12 Å from the iron atom. This barrier agrees with the lack of transitions between closed and open forms of tunnel 1 found in the MD simulations of the monomeric protein (see Figure 8). In contrast, such a barrier is reduced upon dimerization, as the ligand must surpass a barrier of only 2.2 kcal/mol (at about 11 Å from the Fe atom) in *DPgb*-deoxy. The small barrier is followed by a rather flat region between 9 and 6 Å, the latter distance corresponding to the entrance into the distal cavity.

The PMF profile obtained for migration through tunnel 2 in *MPgb*-deoxy is more flat than that obtained for tunnel 1, with a minimum at around 7 Å from the heme, and small barriers (around 1 kcal/mol) that can be easily bypassed due to thermal fluctuations. On the other hand, the most noticeable feature in the PFM profile derived for *DPgb*-deoxy is the appearance of a free energy minimum at around 5 Å, which can be accessed from the bulk solvent through a barrierless migration. Again, these findings agree with the accessibility of ligands through tunnel 2 found in ILS calculations (see Figure 7 and Figure S3 in the Supporting Information).

Overall, SMD simulations point out that, even in the absence of heme-bound  $O_2$ , dimerization plays a substantial role in regulating the migration of ligands through tunnels 1 and 2, leading to enhanced accessibility to the heme in dimeric *MaPgb* compared to the monomeric species.

**Functional Implications.** Inspection of the X-ray structures available for oxygenated (2VEB) and deoxygenated (2VEE) *MaPgb* revealed a number of structural features that are absent in prototypical globins,<sup>14</sup> such as the unusual topology of the two tunnels leading from the distal cavity to the bulk aqueous solvent. It can be anticipated that both tunnels are expected to be functionally relevant since the heme group is completely buried in the interior of *MaPgb*. Even though the biological role of *MaPgb* is still unknown, its biochemical function is likely related to the ability of the branched tunnel to permit the migration of specific ligands. Therefore, understanding the factors that regulate the accessibility of ligands can be of utmost importance in order to shed light into the biological function of *Pgb*.

Support for the biological role of the dimeric *MaPgb* comes from the large contact surface between the two molecules found in the crystallographic unit cell.<sup>14</sup> Gel filtration experiments also suggest that the protein exists as a dimer in solution in a range of concentrations varying from 3 to 100  $\mu\text{M}$ ,<sup>40</sup> thus confirming the previous results reported by Nardini et al.<sup>14</sup> Therefore, it is reasonable to expect that the dimeric form of *MaPgb* will be the physiologically relevant species of the protein. At this point, it is worth noting that our results indicate that access of ligands through the two tunnels is only granted in the dimeric form, as tunnel 1 is primarily closed in the monomer species.

On the other hand, the presence of a dimer might suggest that the protein could exhibit some coupling between the degree of ligation and reactivity. However, recent experimental evidence indicates a lack of any appreciable cooperativity between the interacting subunits for the C(E20)101S mutant.<sup>40</sup> In particular, the absence of significant differences in the CO rebinding kinetics upon changes in the laser pulse energy used in flash photolysis assays strongly argues against the involvement of cooperative effects associated with the assembly state of *MaPgb*.<sup>40</sup> This conclusion is further reinforced by the analysis of CO rebinding kinetics to partially oxygenated *MaPgb*, as the second-order rate constant for CO binding was found to be independent of the fractional  $O_2$  saturation of the dimer, which also rules out a significant cooperativity between subunits (see Figure 3 in ref 40).

The lack of cooperativity effects does not imply that the assembly of the subunits may not influence protein reactivity by affecting the tertiary structure of each monomer. In fact, our results indicate that dimerization has a direct implication on the accessibility of ligands. Thus, whereas tunnel 2 is permanently open along the trajectory of the dimer, there is a balance between open and closed states in tunnel 1 that depend on both dimerization and  $O_2$  binding: in the deoxygenated dimer the closed form is the

major conformational state of tunnel 1, but the open form increases significantly upon O<sub>2</sub> binding to the heme. This effect reflects the net balance of three factors. First, the direct influence exerted by dimerization on the structural arrangement of helix G, which contributes to the interface of the interacting monomers, but also defines, together with helix B, the walls of tunnel 1. Second, the structural and dynamical alteration of helix B upon ligand binding, which is sterically detected by Phe(93)E11. Finally, the steric destabilization of the closed conformation of Phe(145)G8 by the heme-bound O<sub>2</sub>.

On the basis of the preceding discussion, it can be hypothesized that *MaPgb* might be involved in a ligand-controlled bimolecular chemical process, where loading of the protein with a first ligand would facilitate the entry of the second reagent to the heme cavity. This hypothesis is in agreement with experimental findings derived from kinetic studies of CO binding to *MaPgb* in solution and in gels (see Figures 4 and 6 in ref 40), which show that the heterogeneous ligand binding kinetics is affected by ligand concentration.<sup>40</sup> In fact, Abbruzzetti and co-workers have suggested the involvement of a ligand-dependent equilibrium between two conformational species to explain the existence of fast (*MaPgb*<sup>R</sup>) and slow (*MaPgb*<sup>T</sup>) rebinding processes in *MaPgb* (see Figure S5). Notably, analysis of the kinetic phases indicates that, whereas the unliganded protein favors the slow rebinding conformation, ligation favors the fast rebinding phase.

The ligation-dependent transition between slow and fast rebinding conformations is in agreement with the results derived from the simulations here reported, which show that oxygenation of the dimeric *MaPgb* facilitates opening of tunnel 1. The fast and slow rebinding conformations can be interpreted in terms of the open and closed conformational states of Phe(145)G8, which regulates the access through tunnel 1, and of the ligand sensing properties of Phe(93)E11, which contributes to facilitate the transition between closed and open states. Thus, binding of the ligand to the heme is sensed by Phe(93)E11, and the ensuing steric clash alters the protein dynamics by enhancing the flexibility of helices E and B. The increased motility of helix B facilitates the opening of the Phe(145)G8 gate, thus increasing the fraction of proteins in the open conformation, which in turn should enhance the ligand binding rate. Hence, we hypothesize that the fast and slow rebinding conformations of *MaPgb* can be associated with the closed and open forms of the tunnel 1, whose balance is determined by the combined influence of both dimerization (affecting the spatial arrangement of helix G) and ligation (altering the dynamics of helix B).

Clearly, the exploration of mutants that specifically target positions E11 and G8 will be of utmost importance to calibrate the functional role of residues Phe(93)E11 and Phe(145)G8. At present, the X-ray structures of the Tyr(B10)61→Ala and Tyr(B10)61→Trp mutants reveal a significant effect on the accessibility of ligands through tunnel 2.<sup>41</sup> As expected, the Tyr(B10)61→Ala mutant increases the average tunnel diameter by more than 1.5 Å. Nevertheless, this mutation has a profound impact on the relative orientation of Phe(E11)93 and Trp(B9)60, which display two conformations that appear to be correlated to each other. In fact, one of the alternate conformations of Trp(B9)60 partially hinders tunnel 1. On the other hand, the mutation Tyr(B10)61→Trp would reduce the accessibility through tunnel 2, but the partial mobility found for the side chain of this residue suggest that the mutation does not significantly hinder the access of small ligands. However, the mutation has a large effect on the position of Phe(E11)93 and Trp(B9)60 side chains. In fact, the new orientation adopted by

this latter residue hinders the ligand access through tunnel 1. Finally, the analysis of the X-ray structure for the Ile(149)G11→Phe mutant prevents access via tunnel 1, although this effect is triggered by remodeling the side chains of specific distal residues, mainly Trp(B9)60. Overall, these findings suggest that the architecture of the residues in the heme cavity reflects a subtle coupling between side chains, which could be crucial to enhance the sensing properties toward the heme-bound ligand.

In the absence of clear evidence about the nature of the true physiological ligands of *MaPgb*, it is reasonable to expect that a larger ligand (e.g., a triatomic molecule) could lead to a more effective opening of tunnel 1 due to enhanced steric hindrance with the sensing Phe residues. Accordingly, the balance between open and closed states might be regulated by the size/polarity of the ligand, so that opening of tunnel 1 might be facilitated upon binding of an incoming compound through tunnel 2, thus paving the way for the involvement of *MaPgb* in mediating a bimolecular chemical process. Finally, our results indicate that dimerization might represent a mechanism to regulate the functional role of *MaPgb*, with the dimeric state being required to attain the biologically relevant form of the protein.

## CONCLUSIONS

The structural analysis of the MD simulations run for deoxy- and oxygenated states of monomeric and dimeric *MaPgb*, and the energetic characterization of the tunnels identified in the X-ray structure reveals a number of factors potentially important for the biological role of the protein. First, the absence of stabilizing interactions between the heme-bound O<sub>2</sub> and distal residues reinforces the hypothesis that observed striking distortion of the heme porphyrin ring plays a key role on O<sub>2</sub> affinity. Moreover, the accessibility of ligands through tunnel 1 appears to be regulated by the side chain of Phe(145)G8, which can adopt two different conformations. The balance between open and closed states is affected by the synergistic effect of two main factors: (i) attainment of a dimeric protein, and (ii) the presence of the heme-bound ligand. By contrast, binding of O<sub>2</sub> to a hypothetical monomeric form of the protein is found to have minor impact on the accessibility of tunnel 1. On the basis of these results, it might be hypothesized that *MaPgb* is involved in a ligand-regulated bimolecular process, where binding of a ligand accessing the heme cavity through tunnel 2 would facilitate the migration of a second reagent through tunnel 1, thus leading to an overall increase in the reactivity of the protein.

## ASSOCIATED CONTENT

**S Supporting Information.** Specific parameters for the heme in Pgb, conformational preferences of sensing residues Phe(93)E11 and Phe(145)G8, and free energy isosurfaces used to delineate tunnels 1 and 2 in Pgb. This material is available free of charge via the Internet at <http://pubs.acs.org>.

## AUTHOR INFORMATION

### Corresponding Author

\*E-mail: [fjluque@ub.edu](mailto:fjluque@ub.edu) (F.J.L.); [dario@qi.fcen.uba.ar](mailto:dario@qi.fcen.uba.ar) (D.E.).

## ACKNOWLEDGMENT

This work was partially supported by the University of Buenos Aires, ANPCyT, CONICET, the Spanish Ministerio de Innovación y

Ciencia (SAF2008-05595, PCI2006-A7-0688, IT2009-0010), the Generalitat de Catalunya (2009-SGR00298), Azioni Integrate Italia Spagna 2009 (IT10L1M59M), and the EU FP7 program (project NOstress). This project was supported by the Italian Ministero dell'Istruzione, dell'Università e della Ricerca (MIUR), Direzione Generale per l'Internazionalizzazione della Ricerca, Progetti di Grande Rilevanza Italia-Argentina. F.F. received a fellowship from the Spanish Ministerio de Innovación y Ciencia. Computational facilities provided by the Barcelona Supercomputer Center and the Centre de Supercomputació de Catalunya are acknowledged.

## REFERENCES

- (1) *The Smallest Biomolecules: Diatomics and Their Interactions with Heme Proteins*; Ghosh, A., Ed.; Elsevier: Amsterdam, 2007.
- (2) Paoli, M.; Marles-Wright, J.; Smith, A. *DNA Cell Biol.* **2002**, *21*, 271–280.
- (3) Vinogradov, S. N. M.; Moens, L. *J. Biol. Chem.* **2008**, *283*, 8773–8777.
- (4) Frauenfelder, H.; McMahon, B. H.; Fenimore, P. W. *Proc. Natl. Acad. Sci. U.S.A.* **2003**, *100*, 8615–8617.
- (5) Scott, E. E.; Gibson, Q. H.; Olson, J. S. *J. Biol. Chem.* **2001**, *276*, 5177–5188.
- (6) Wittenberg, J. B.; Wittenberg, B. A. *J. Exp. Biol.* **2003**, *206*, 2011–2020.
- (7) Kapp, O. H.; Moens, L.; Vanfleteren, J.; Trotman, C. N.; Suzuki, T.; Vinogradov, S. N. *Protein Sci.* **1995**, *4*, 2179–2190.
- (8) Nardini, M.; Pesce, A.; Milani, M.; Bolognesi, M. *Gene* **2007**, *398*, 2–11.
- (9) Wittenberg, J. B.; Bolognesi, M.; Wittenberg, B. A.; Guertin, M. *J. Biol. Chem.* **2002**, *277*, 871–874.
- (10) Freitas, T. A. K.; Hou, S.; Dioum, E. M.; Saito, J. A.; Newhouse, J.; Gonzalez, G.; Gilles-Gonzalez, M.-A.; Alam, M. *Proc. Natl. Acad. Sci. U.S.A.* **2004**, *101*, 6675–6680.
- (11) Hou, S.; Freitas, T.; Larsen, R. W.; Piatibratov, M.; Sivozhelzov, V.; Yamamoto, A.; Meleshkevitch, E. A.; Zimmer, M.; Ordal, G. W.; Alam, M. *Proc. Natl. Acad. Sci. U.S.A.* **2001**, *98*, 9353–9358.
- (12) Vinogradov, S.; Hoogewijs, D.; Bailly, X.; Arredondo-Peter, R.; Gough, J.; Dewilde, S.; Moens, L.; Vanfleteren, J. *BMC Evol. Biol.* **2006**, *6*, 31–47.
- (13) Vinogradov, S. N.; Hoogewijs, D.; Bailly, X.; Mizuguchi, K.; Dewilde, S.; Moens, L.; Vanfleteren, J. R. *Gene* **2007**, *398*, 132–142.
- (14) Nardini, M. P. A.; Thijs, L.; Saito, J. A.; Dewilde, S.; Alam, M.; Ascenzi, P.; Coletta, M.; Ciaccio, C.; Moens, L.; Bolognesi, M. *EMBO Rep.* **2008**, *9*, 157–163.
- (15) Martí, M. A.; Crespo, A.; Capece, L.; Boechi, L.; Bikiel, D. E.; Scherlis, D. A.; Estrin, D. A. *J. Inorg. Biochem.* **2006**, *100*, 761–770.
- (16) Ruscio, J. Z.; Kumar, D.; Shukla, M.; Prisant, M. G.; Murali, T. M.; Onufriev, A. V. *Proc. Natl. Acad. Sci. U.S.A.* **2008**, *105*, 9204–9209.
- (17) D'Abramo, M.; Di Nola, A.; Amadei, A. *J. Phys. Chem. B* **2009**, *113*, 16346–16353.
- (18) Wang, P.; Best, R. B.; Blumberger, J. *Phys. Chem. Chem. Phys.* **2011**, *13*, 7708–7719.
- (19) Nienhaus, K.; Dominici, P.; Astegno, A.; Abbruzzetti, S.; Viappiani, C.; Nienhaus, G. U. *Biochemistry* **2010**, *49*, 7448–7458.
- (20) Guallar, V.; Wallrapp, F. H. *Biophys. Chem.* **2010**, *149*, 1–11.
- (21) Cohen, J.; Schulten, K. *Biophys. J.* **2007**, *93*, 3591–3600.
- (22) Ceccarelli, M.; Anedda, R.; Casu, M.; Ruggerone, P. *Proteins* **2007**, *71*, 1231–1236.
- (23) Tomita, A.; Sato, T.; Ichiyangi, K.; Nozawa, S.; Ichikawa, H.; Chollet, M.; Kawai, F.; Park, S.-Y.; Tsuduki, T.; Yamato, T.; Koshihara, S.-Y.; Adaci, S.-I. *Proc. Natl. Acad. Sci. U.S.A.* **2009**, *106*, 21612–22616.
- (24) Jorgensen, W.; Chandrasekhar, J.; Madura, J.; Impey, R.; Klein, M. *J. Chem. Phys.* **1983**, *79*, 926–935.
- (25) Darden, T.; York, D.; Pederson, L. *J. Chem. Phys.* **1993**, *98*, 10089–10092.
- (26) Ryckaert, J.-P.; Ciccotti, G.; Berendsen, H. J. C. *J. Comput. Phys.* **1977**, *23*, 327–341.
- (27) Hornak, V.; Abel, R.; Okur, A.; Strockbine, B.; Roitberg, A.; Simmerling, C. *Proteins* **2006**, *65*, 712–725.
- (28) Boechi, L.; Martí, M. A.; Milani, M.; Bolognesi, M.; Luque, F. J.; Estrin, D. A. *Proteins* **2008**, *73*, 372–379.
- (29) Boechi, L.; Manez, P. A.; Luque, F. J.; Martí, M. A.; Estrin, D. A. *Proteins* **2009**, *78*, 962–970.
- (30) Case, D.; Darden, T. A.; Cheatham, T. E., III; Simmerling, C. L.; Wang, J.; Duke, R. E.; Luo, R.; Merz, K. M.; Pearlman, D. A.; Crowley, M.; Walker, R. C.; Zhang, W.; Wang, B.; Hayik, S.; Roitberg, A.; Seabra, G.; Wong, K. F.; Paesani, F.; Wu, X.; Brozell, S.; Tsui, V.; Gohlke, H.; Yang, L.; Tan, C.; Mongan, J.; Hornak, V.; Cui, G.; Beroza, P.; Matthews, D. H.; Schafmeister, C.; Ross, W. S.; Kollman, P. A. *AMBER*, version 9; University of California: San Francisco, CA, 2006.
- (31) Cohen, J.; Arkhipov, A.; Braun, R.; Schulten, K. *Biophys. J.* **2006**, *91*, 1844–1857.
- (32) Forti, F.; Boechi, L.; Estrin, D. A.; Martí, M. A. *J. Comput. Chem.* **2011**, *32*, 2219–2231.
- (33) Jarzynski, C. *Phys. Rev. Lett.* **1997**, *78*, 2690–2693.
- (34) Martí, M. A.; Bidon-Chanal, A.; Crespo, A.; Yeh, S.-R.; Guallar, V.; Luque, F. J.; Estrin, D. A. *J. Am. Chem. Soc.* **2008**, *130*, 1688–1693.
- (35) García, A. *Phys. Rev. Lett.* **1992**, *68*, 2696–2699.
- (36) Amadei, A.; Linssen, A. B.; Berendsen, H. J. C. *Proteins* **1993**, *17*, 412–425.
- (37) Crespo, A.; Martí, M. A.; Kalko, S. G.; Morreale, A.; Orozco, M.; Gelpi, J. L.; Luque, F. J.; Estrin, D. A. *J. Am. Chem. Soc.* **2005**, *127*, 4433–4444.
- (38) Mukai, M. O.; Ouellet, Y.; Ouellet, H.; Guertin, M.; Yeh, S. R. *Biochemistry* **2004**, *43*, 2764–2770.
- (39) Bikiel, D. E.; Boechi, L.; Nardini, M.; Luque, F. J.; Martí, M. A.; Estrin, D. A. *J. Phys. Chem. B* **2010**, *114*, 8536–8543.
- (40) Abbruzzetti, S.; Tillemann, L.; Bruno, S.; Viappiani, C.; Desmet, F.; van Doorslaer, S.; Coletta, M.; Ciaccio, C.; Ascenzi, P.; Moens, L.; Dewilde, S.; Viappiani, C. *PLoS One*, submitted for publication.
- (41) Pesce, A.; Tillemann, L.; Dewilde, S.; Ascenzi, P.; Coletta, M.; Ciaccio, C.; Bruno, S.; Moens, L.; Bolognesi, M.; Nardini, M. *IUBMB Life* **2011**, *63*, 287–294.